Research Article | Vol. 25, No. 16 | 7 Aug 2017 | OPTICS EXPRESS 19548
Optics EXPRESS

Comparison between broadband Bessel beam launchers based on either Bessel or Hankel aperture distribution for millimeter wave short pulse generation

SANTI C. PAVONE,[1,*] AGNESE MAZZINGHI,[2] ANGELO FRENI,[2] AND MATTEO ALBANI[1]

[1]*Department of Information Engineering and Mathematics, University of Siena, 53100 Siena, Italy*
[2]*Department of Information Engineering, University of Florence, 50139 Florence, Italy*
[*]*santi.pavone@unisi.it*

Abstract: In this paper, a comparison is presented between Bessel beam launchers at millimeter waves based on either a cylindrical standing wave (CSW) or a cylindrical inward traveling wave (CITW) aperture distribution. It is theoretically shown that CITW launchers are better suited for the generation of electromagnetic short pulses because they maintain their performances over a larger bandwidth than those realizing a CSW aperture distribution. Moreover, the wavenumber dispersion of both the launchers is evaluated both theoretically and numerically. To this end, two planar Bessel beam launchers, one enforcing a CSW and the other enforcing a CITW aperture distribution, are designed at millimeter waves with a center operating frequency of $f = 60$ GHz and analyzed in the bandwidth $50 - 70$ GHz by using an in-house developed numerical code to solve Maxwell's equations based on the method of moments. It is shown that a monochromatic Bessel beam can be efficiently generated by both the launchers over a wide fractional bandwidth. Finally, we investigate the generation of limited-diffractive electromagnetic pulses at millimeter waves, up to a certain non-diffractive range. Namely, it is shown that by feeding the launcher with a Gaussian short pulse, a spatially confined electromagnetic pulse can be efficiently generated in front of the launcher.

OCIS codes: (050.1220) Apertures; (090.0090) Holography; (050.0050) Diffraction and gratings; (080.0080) Geometric optics; (350.7420) Waves; (350.5500) Propagation.

References and links

1. H. E. Hernandez-Figueroa, M. Zamboni-Rached, and E. Recami, *Localized Waves* (J. Wiley & Sons, 2008).
2. H. E. Hernandez-Figueroa, E. Recami, M. Zamboni-Rached, *Non-Diffracting Waves* (J. Wiley & Sons, 2013).
3. P. Saari, K. Reivelt, "Generation and classification of localized waves by Lorentz transformations in Fourier space," Phys. Rev. E **69**, 036612 (2004).
4. J. Durnin, J. J. Miceli Jr., and J. H. Eberly, "Diffraction-free beams," Phys. Rev. Lett. **58**, 1499–1501 (1987).
5. J. Arlt and K. Dholakia, "Generation of high-order Bessel-beams by use of an axicon," Opt. Comm. **177**, 297 (2000).
6. O. Brzobohaty, T. Cizmár, and P. Zemánek, "High quality quasi-Bessel beam generated by round-tip axicon," Opt. Expr. **16**(17), 12688–12700 (2008).
7. M. Ettorre and A. Grbic, "Generation of propagating Bessel beams using leaky-wave modes," IEEE Trans. Anten. Propag. **60**, 3605–3613 (2012).
8. W. Fuscaldo, G. Valerio, A. Galli, R. Sauleau, A. Grbic, and M. Ettorre, "Higher-Order Leaky-Mode Bessel-Beam Launcher," IEEE Trans. Antennas Propag. **64**(3), 904–913 (2015).
9. S. C. Pavone, M. Ettorre, and M. Albani, "Analysis and Design of Bessel Beam launchers: Longitudinal Polarization," IEEE Trans. Anten. Propag. **22**(6), 2311–2318 (2016).
10. J. N. Brittingham,"Focus Wave Modes in homogeneous Maxwell's equations: Transverse electric mode," Journ. Appl. Phys. **54**, 1179 (1983).
11. R. Ziolkowski, "Exact Solutions of the Wave Equation with Complex Source Locations," J. Math. Phys. **26**, 861 (1985).
12. E. Heyman, L. Felsen, and B. Steinberg, "Spectral Analysis of Focus Wave Modes," J. Opt. Soc. Am. A **4**, 2081 (1987).
13. E. Heyman and L. Felsen, "Complex-source Pulsed-beam Fields," J. Opt. Soc. Am. A, **6**, 806 (1989).

#296205 https://doi.org/10.1364/OE.25.019548
Journal © 2017 Received 17 May 2017; revised 18 Jul 2017; accepted 18 Jul 2017; published 4 Aug 2017

Optics EXPRESS

14. R. Ziolkowski, "Aperture Realizations of Exact Solutions to Homogeneous Wave Equations," J. Opt. Soc. Am. A **10**, 75 (1993).
15. P. Saari, and K. Reivelt, "Evidence of X-shaped propagation-invariant localized light waves," Phys. Rev. Lett. **79**, 4135 (1997).
16. R. Ziolkowski, I. M. Besieris, A. M. Shaarawi, "On the superluminal propagation of X-shaped localized waves," J. Phys. A: Math. Gen. **33**, 7227–7254 (2000).
17. K. Reivelt, and P. Saari, "Optical generation of focus wave modes," J. Opt. Soc. Am. A **17**, 1785–1790 (2000).
18. I. Alexeev, K. Y. Kim, and H. M. Milchberg, "Measurement of the Superluminal Group Velocity of an Ultrashort Bessel Beam Pulse," Phys. Rev. Lett. **88**, 073901 (2002).
19. K. Reivelt, and P. Saari, "Experimental demonstration of realizability of optical focus wave modes," Phys. Rev. E **66**, 056611 (2002).
20. R. Grunwald, V. Kebbel, U. Griebner, U. Neumann, A. Kummrow, M. Rini, E. T. J. Nibbering, M. Piché, G. Rousseau, and M. Fortin, "Generation and characterization of spatially and temporally localized few-cycle optical wave packets," Phys. Rev. A **67**(6), 063820 (2003).
21. R. Grunwald, T. Elsaesser, and M. Bock, "Spatio-Temporal Coherence Mapping of Few-Cycle Vortex Pulses," Sci. Rep. **4**, 7148 (2014).
22. D. Comite, W. Fuscaldo, S. C. Pavone, G. Valerio, M. Ettorre, M. Albani, and A. Galli, "Propagation of nondiffracting pulses carrying orbital angular momentum at microwave frequencies," Appl. Phys. Lett. **110**, 114102 (2017).
23. P. Bowlan, H. Valtna-Lukner, M. Lohmus, P. Piksarv, P. Saari, and R. Trebino, "Measuring the spatiotemporal field of ultrashort Bessel-X pulses," Opt. Lett. **34**(15), 2276–2278 (2009).
24. M. Lohmus, P. Bowlan, P. Piksarv, H. Valtna-Lukner, R. Trebino, and P. Saari, "Diffraction of ultrashort optical pulses from circularly symmetric binary phase gratings," Opt. Lett. **37**(7), 1238–1240 (2012).
25. M. Albani, S. C. Pavone, M. Casaletti, and M. Ettorre, "Generation of non-diffractive Bessel beams by inward cylindrical traveling wave aperture distribution," Opt. Expr. **22**, 18354–18364 (2014).
26. S. C. Pavone, M. Ettorre, M. Casaletti, and M. Albani, "Transverse circular-polarized Bessel beam generation by inward cylindrical aperture distribution," Opt. Expr. **24**(10), 11103–11111 (2016).
27. A. Mazzinghi, M. Balma, D. Devona, G. Guarnieri, G. Mauriello, M. Albani, and A. Freni, "Large Depth of Field Pseudo-Bessel Beam Generation with a RLSA Antenna," IEEE Trans. Anten. Propag **62**, 3911–3919 (2014).
28. C. A. Balanis, *Antenna theory: analysis and design*, (Wiley, 2016).
29. W. Fuscaldo, S. C. Pavone, G. Valerio, A. Galli, M. Albani, and M. Ettorre, "Analysis of limited-diffractive and limited-dispersive X-waves generated by finite radial waveguides," J. Appl. Phys. **119**(19), 194903 (2016)
30. M. Albani, A. Mazzinghi, and A. Freni, "Automatic design of CP-RLSA antennas," IEEE Trans. Anten. Propag. **60**, 5538–5547 (2012).
31. H. Bethe, "Theory of Diffraction by Small Holes," Phys. Rev. **66**, 163 (1944).
32. C. A. Balanis, *Advanced Engineering Electromagnetics* (John Wiley & Sons, 2012).
33. M. Abramowitz, and I. Stegun, *Handbook of Mathematical functions* (Dover, 1965).
34. R. F. Harrington, *Field Computation by Moment Methods* (Wiley-IEEE, 1993).
35. M. Albani, G. La Cono, R. Gardelli, and A. Freni, "An efficient full-wave method of moments analysis for RLSA antennas," IEEE Trans. Anten. Propag. **54**(8), 2326–2336 (2006).

1. Introduction

In recent years, localized waves [1, 2] have gained increasing interest among researchers, because of their remarkable property of being non-diffractive, i.e. their transverse field profile theoretically does not spread out up to a certain distance called depth of field (DOF) or non-diffractive range [3]. From the theoretical viewpoint, they are monochromatic solutions of Helmholtz equation and, among them, Bessel beams can be undoubtedly considered ones of the most renowned, since their early introduction by Durnin [4].

Several attempts have been made to practically realize Bessel beams launchers, both at optical [5, 6] and at radio [7–9] frequencies. Polychromatic solutions to Helmholtz equation can be obtained as a continuous superposition of monochromatic solutions on a certain frequency bandwidth. They have also been considered for the generation of localized pulses [10–20], i.e. efficiently spatially confined electromagnetic (EM) pulses. Such pulses can also produce *optical vortices* and a non-null orbital angular momentum (OAM), when an azimuthal phase variation of the aperture field is introduced [21, 22]. At optical frequencies, common Bessel beam generators used to produce broadband pulses are axicons and binary phase gratings, which generate *superluminal* or *subluminal* wave-packets, respectively [23, 24].

In this paper, we propose a comparative broadband analysis of two different approaches to

Optics EXPRESS

generate EM pulses at millimeter waves by using a Radial Line Slot Array (RLSA); namely, by synthesizing either a cylindrical inward traveling wave (CITW) [9,25,26] or a cylindrical standing wave (CSW) [27] aperture distribution, whose respective mathematical description is an Hankel or a Bessel function, respectively. It is worth noting that the proposed EM pulse launchers do not generate vortices and OAM at millimeter waves, since the overall phase progression of the synthesized field distribution is constant on the radiating aperture.

Since for RLSA antennas the impedance bandwidth (i.e., the frequency range in which the device can efficiently accepts the input power from the feeder, normally a coaxial cable at microwaves/millimeter waves) is usually very large, the band limitation of the device is then mainly caused by the aperture distribution deterioration out of the central design frequency. For a Bessel beam launcher, unlike standard antennas, the gain is not a useful parameter to characterize performances and bandwidth, since it is normally well-defined for applications in the Fraunhofer (or far-field) region [28]. On the other hand, the spatial confinement of the generated EM pulses, both in the longitudinal and transverse directions with respect to the axis of propagation, is connected to the launcher dispersion characteristic and, therefore, it will be investigated in detail. It has been shown in [29] that the bandwidth of the feeding pulse plays a key-role in the longitudinal confinement of the pulse, whereas Bessel beam beamwidth at the central frequency dictates the transverse confinement of the pulse. To make a balanced comparison, both CITW and CSW launchers are analyzed when fed by a Gaussian pulse, and the spatial dispersion of generated EM pulses is examined, revealing a *subluminal* weakly-dispersive propagation up to the DOF.

The proposed comparison clarifies strong points and intrinsic limitations of both RLSA CSW and CITW launchers for the efficient generation of EM pulses at millimeter waves.

2. Analysis of broadband response of RLSA Bessel beam launchers

In this Section, an approximate model is derived for the estimation of RLSA Bessel beam launchers dispersion properties (i.e., the wavenumber versus frequency diagram), either in the case of CITW or CSW aperture distributions. In the following, the standard cylindrical reference system (ρ, ϕ, z) is considered, with the origin lying at the center of the radiating aperture corresponding to the plane $z = 0$. The launchers are made by conveniently etching several slot pairs on the top plate of a radial parallel plate waveguide (PPW), so as to synthesize the desired CSW or CITW magnetic current distribution, by using a holographic criterion [30]. According to Bethe theory [31], each slot can be modeled as an equivalent magnetic dipole moment, whose strength is proportional to the incident magnetic field $\mathbf{H}^{inc}$ of the feeding wave (which propagates inside the PPW) at the slot position, namely

$$\mathbf{M} = \underline{\boldsymbol{\alpha}} \cdot \mathbf{H}^{inc}, \tag{1}$$

where $\underline{\boldsymbol{\alpha}}$ is the dyadic slot polarizability, that is dominantly directed along the slot direction $\hat{\mathbf{u}}_s$ for a single slot ($\underline{\boldsymbol{\alpha}} \approx \alpha \hat{\mathbf{u}}_s \hat{\mathbf{u}}_s$), whereas it is given by $\underline{\boldsymbol{\alpha}} \approx \alpha(e^{j\pi/4}\hat{\mathbf{u}}_1\hat{\mathbf{u}}_1 + e^{-j\pi/4}\hat{\mathbf{u}}_2\hat{\mathbf{u}}_2)$, with $\hat{\mathbf{u}}_{1,2} = (\hat{\boldsymbol{\phi}} \mp \hat{\boldsymbol{\rho}})/\sqrt{2}$, for a right/left handed circular polarized slot pair (RH/LHCP) [30]. Without loss of generality, here we will focus on the RHCP case. Moreover, we suppose the PPW to be fed by the fundamental TM^{00} Transverse Magnetic mode. Hence, the magnetic field incident on each slot (on the PPW side) is [32]

$$\mathbf{H}^{inc}(\rho, \phi) = AH_1^{(2)}(k_d\rho)\hat{\boldsymbol{\phi}}, \tag{2}$$

where $k_0 = 2\pi f/c$ and $k_d = k_0\sqrt{\epsilon_r}$ are the wavenumbers in free-space and in the dielectric filling the PPW, respectively, $H_n^{(m)}(\cdot)$ is the m-th kind Hankel function of n-th order, and A is an arbitrary amplitude constant. By asymptotically evaluating Eq. (2) for large arguments

Optics EXPRESS

($k_d\rho >> 1$) [33], one finds the cylindrical wave expression

$$\mathbf{H}^{inc}(\rho,\phi) \approx jA\sqrt{\frac{2j}{k_d\pi}}\frac{e^{-jk_d\rho}}{\sqrt{\rho}}\hat{\boldsymbol{\phi}} \tag{3}$$

and then the RLSA slot pair dipole moment can be estimated as

$$\mathbf{M}(\rho,\phi) \approx \alpha A\sqrt{\frac{2j}{k_d\pi}}\frac{e^{-j(k_d\rho-\phi)}}{\sqrt{\rho}}\hat{\mathbf{u}}_{RH}, \tag{4}$$

where $\hat{\mathbf{u}}_{RH} = (\hat{\mathbf{x}} - j\hat{\mathbf{y}})/\sqrt{2}$ denotes the RHCP unit vector. The above formula is used to design the desired aperture distribution. Indeed, the magnetic dipole moment phase is selected by the slot pair positions (ρ,ϕ), whereas its amplitude is modulated by the slot length, which in turn modulates the slot polarizability α [30].

In the next subsections, the previous results will be specialized for the cases of CSW and CITW magnetic current distributions.

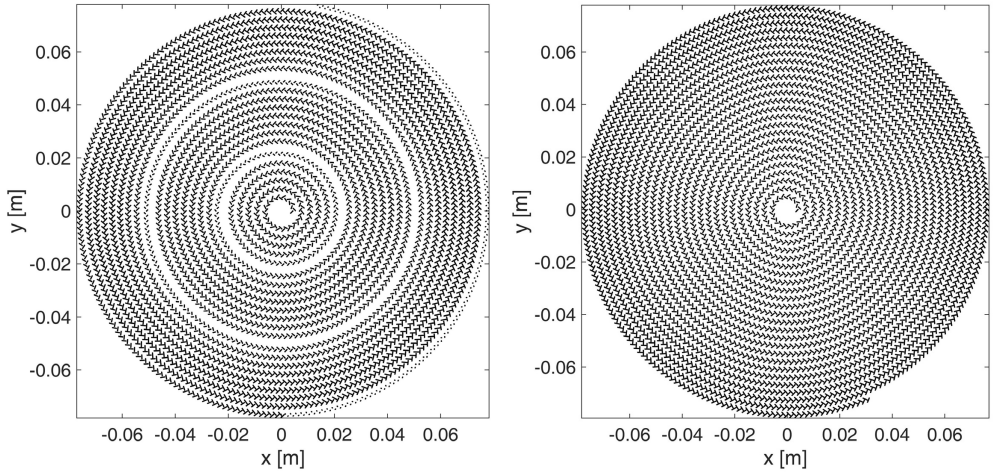

Fig. 1. Design of Bessel beam launchers implementing (a) CSW and (b) CITW aperture distributions.

2.1. Launcher based on a cylindrical standing wave aperture distribution

As presented in [27], a RLSA Bessel beam launcher based on a CSW can be designed by synthesizing a magnetic dipole moment distribution at the center operating frequency $f = \bar{f}$ (hereinafter a bar over a quantity denotes that it is evaluated at the design frequency $\bar{f}$)

$$\mathbf{M}(\rho,\phi) = 2M_0 J_0\left(\bar{k}_\rho\rho\right)\hat{\mathbf{u}}_{RH}, \tag{5}$$

in which $\bar{k}_\rho = \bar{k}_0\sin\bar{\theta}$ is the imposed radial wavenumber and $\bar{\theta}$ the corresponding axicon angle at the design frequency, $J_0(\cdot)$ the zeroth order Bessel function, and M_0 is an arbitrary constant amplitude. By equating the magnitudes of Eq. (5) and Eq. (4), one finds the shaping of the polarizability α

$$\alpha \approx \left|\frac{M_0}{A}\right|\sqrt{2\pi\bar{k}_d\rho}\left|J_0(\bar{k}_\rho\rho)\right| \approx 2\left|\frac{M_0}{A}\cos\left(\bar{k}_\rho\rho - \frac{\pi}{4}\right)\right|, \tag{6}$$

Optics EXPRESS

which can be achieved by a suitable shaping of the slot lengths. To set Eq. (6) equal to Eq. (4), also the phase has to be the same. Therefore, the positions of slot pairs have to be chosen alternatively on the two spirals $\rho = \rho_0 + \phi/\bar{k}_d$ and $\rho = \rho_0 + \phi/\bar{k}_d + \bar{\lambda}_d/2$ (being ρ_0 an arbitrary starting point close to the antenna center, and $\bar{\lambda}_d = \lambda_0/\sqrt{\epsilon_r}$ the wavelength in the dielectric filling the PPW at the design frequency), to achieve the required π phase shift across the Bessel function zeros, as shown in Fig. 1(a).

To analyze the broadband behavior of such a Bessel beam launcher based on a CSW aperture distribution, let us vary the operating frequency f of an amount $\Delta f = f - \bar{f}$. Since the slot positions are fixed by the design performed at $\bar{f}$, then the equivalent magnetic current distribution becomes

$$\mathbf{M}(\rho, \phi) \approx 2M_0 J_0(\bar{k}_\rho \rho) e^{-j\Delta k_d \rho} \hat{\mathbf{u}}_{RH}, \tag{7}$$

in which the wavenumber variation $\Delta k_d = k_d - \bar{k}_d = 2\pi \Delta f \sqrt{\epsilon_r}/c$ has been introduced. Indeed, the frequency shift introduces a radial linear phasing on the aperture. By decomposing the Bessel function in Eq. (7) as the sum of two Hankel functions, namely $2J_0(\bar{k}_\rho \rho) = H_0^{(1)}(\bar{k}_\rho \rho) + H_0^{(2)}(\bar{k}_\rho \rho)$, two wave contributions are highlighted. The first wave constituent is an inward traveling wave with a radial wavenumber $k_\rho = -\bar{k}_\rho + \Delta k_d$ radiating a geometrical optics (GO) field, inside a cone around the z-axis with tip coinciding with the launcher center [26], which is a Bessel beam with transverse electric field

$$\mathbf{E}_t(\rho, \phi, z) \approx 2M_0 J_0\left((\bar{k}_\rho - \Delta k_d)\rho\right) e^{-j\sqrt{k_0^2 - (\bar{k}_\rho - \Delta k_d)^2} z} \hat{\mathbf{u}}_{RH}. \tag{8}$$

Such a contribution is no longer present if the frequency becomes greater than $f \geq \bar{f}\left(1 + \sin\bar{\theta}/\sqrt{\epsilon_r}\right)$, since the radial wavenumber becomes positive, hence the inward Hankel wave contribution becomes an outward one [25, 26]. On the other hand, the second wave constituent is an outward traveling wave aperture distribution with a radial wavenumber $k_\rho = \bar{k}_\rho + \Delta k_d$, that contributes only to the diffracted field and does not radiate any leading GO contribution. However, for frequencies below the design frequency $\bar{f}$ such that $f \leq \bar{f}\left(1 - \sin\bar{\theta}/\sqrt{\epsilon_r}\right)$, this wave becomes an inward Hankel wave, and an additional GO field contribution arises inside the cone $\theta < \bar{\theta}$, hence the total transverse electric field is the superposition of two Bessel beams

$$\begin{aligned}\mathbf{E}_t(\rho, \phi, z) \approx 2M_0 \Big[& J_0\left((\bar{k}_\rho - \Delta k_d)\rho\right) e^{-j\sqrt{k_0^2 - (\bar{k}_\rho - \Delta k_d)^2} z} + \\ & J_0\left((\bar{k}_\rho + \Delta k_d)\rho\right) e^{-j\sqrt{k_0^2 - (\bar{k}_\rho + \Delta k_d)^2} z} \Big] \hat{\mathbf{u}}_{RH}.\end{aligned} \tag{9}$$

In conclusion, a pure Bessel beam can be generated by using a standing cylindrical aperture distribution, such as that depicted in Fig. 2(a), only in the frequency range

$$\bar{f}\left(1 - \sin\bar{\theta}/\sqrt{\epsilon_r}\right) \leq f \leq \bar{f}\left(1 + \sin\bar{\theta}/\sqrt{\epsilon_r}\right). \tag{10}$$

2.2. Launcher based on an inward traveling wave aperture distribution

As outlined in [26], a proper slot arrangement shown in Fig. 1(b) allows for the synthesis of a RLSA Bessel beam launcher based on a CITW distribution of the form

$$\mathbf{M}(\rho, \phi) = M_0 H_0^{(1)}\left(\bar{k}_\rho \rho\right) \hat{\mathbf{u}}_{RH}, \tag{11}$$

at the design frequency $\bar{f}$. Such an aperture distribution is achieved by choosing the slot lengths by comparing Eq. (11) and Eq. (4), so that

$$\alpha \approx \left|\frac{M_0}{A}\right| \sqrt{\frac{\bar{k}_d}{\bar{k}_\rho}}, \tag{12}$$

Optics EXPRESS

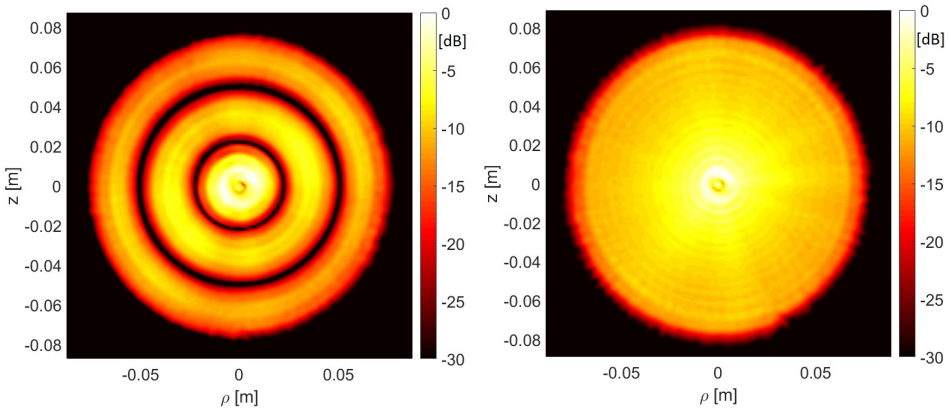

Fig. 2. Synthesized co-polar component of the electric field for both (a) CSW and (b) CITW launchers, evaluated on a plane at $z = \lambda_0 = 5$ mm, at the central frequency $f = 60$ GHz.

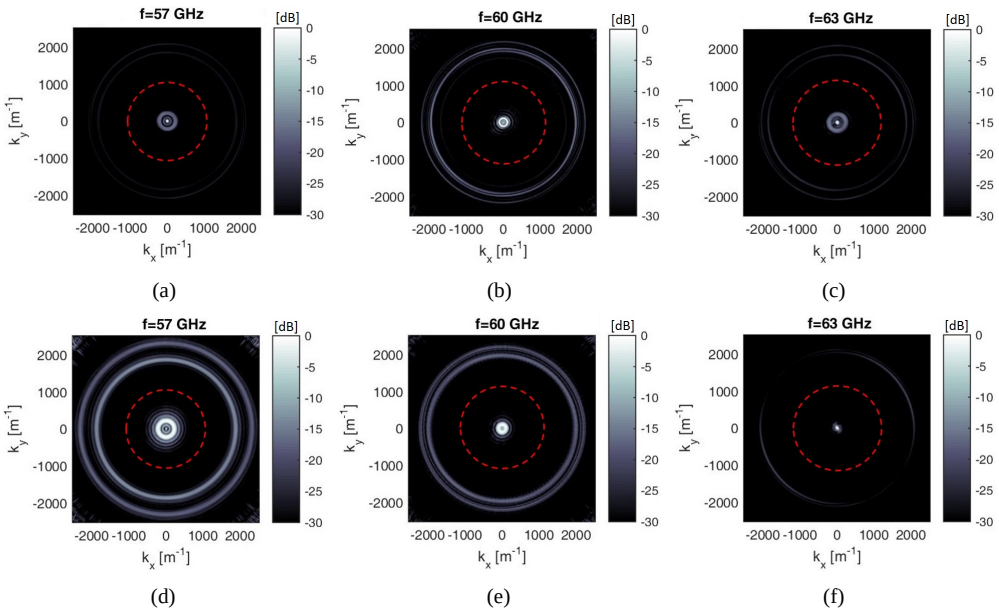

Fig. 3. Transverse wavenumber spectrum for (a,b,c) CSW and (d,e,f) CITW launchers, at $f = 57$ GHz, 60 GHz and 63 GHz, respectively. The *visible* limit is highlighted in each plot (dashed red lines).

Optics EXPRESS

and their position is on the spiral $\rho = \rho_0 + \phi / \left(\bar{k}_d + \bar{k}_\rho\right)$. If a deviation from the central frequency is imposed, the different phase progression on the aperture gives

$$\mathbf{M}(\rho, \phi) \approx M_0 H_0^{(1)}\left(\bar{k}_\rho \rho\right) e^{-j\Delta k_d \rho} \hat{\mathbf{u}}_{RH}, \tag{13}$$

where, again, a linear phasing is induced on the aperture. By the same considerations as in the previous subsection, when the frequency becomes greater than $\bar{f}\left(1 + \sin\bar{\theta}/\sqrt{\epsilon_r}\right)$ the inward traveling wave aperture distribution becomes outward, and, according to [26], no Bessel beam can be generated inside the cone $\theta < \bar{\theta}$. Thus, a Bessel beam in the same form of Eq. (8) is generated by the CITW aperture distribution in the frequency range

$$f \leq \bar{f}\left(1 + \sin\bar{\theta}/\sqrt{\epsilon_r}\right). \tag{14}$$

It is worth noting that such a frequency range has the same upper-bound of that in Eq. (10), but does not have any lower-bound. Hence, CITW launchers exhibit better performances in terms of operating bandwidth, and do not suffer of the occurrence of an additional spurious Bessel beam at low frequency.

3. Design of CSW and CITW Bessel beam launchers

In this Section, we compare the broadband capabilities of two different practical Bessel beam launchers in RLSA technology, obtained by enforcing a CSW and a CITW aperture distribution. Both the launchers are designed at the central frequency $\bar{f} = 60$ GHz, by assuming an aperture of radius $\rho_a = 15.5\bar{\lambda} = 78.5$ mm, and an *axicon* angle $\bar{\theta} = \arcsin(\bar{k}_\rho/\bar{k}) = 5°$, being $\bar{\lambda} = 5$ mm the wavelength at the design frequency and $\bar{k}_\rho = \bar{k}\sin\bar{\theta} \approx 109$ m^{-1} the radial wavenumber imposed on the aperture. All slot pairs center are spaced $\Delta S = 0.7\bar{\lambda} = 3.5$ mm each other along the spiral. Both the launchers radiate a right-hand circular polarization (RHCP).

The radial PPW with relative permittivity of the filling dielectric $\epsilon_r = 2.2 - j(1.98 \times 10^{-3})$, and thickness $h = 7.87$ mm was designed to allow the propagation of only the fundamental TM^{00} mode. The starting design has been calculated according to the simplified model described in Section 2, then an in-house method of moments was used for the EM analysis [34,35] and for the launcher optimization until its aperture field fits the desired one [30]. The synthesized co-polar (RHCP) component of the electric field was evaluated for both the launchers on an aperture plane at $z = \bar{\lambda}_0 = 5$ mm and reported in Fig. 2, exhibiting a substantial azimuthal symmetry and following the desired Bessel or Hankel function shape, as expected from Eqs. (5)–(11).

3.1. Transverse wavenumber spectral analysis

To derive the dispersion properties of the synthesized launchers, a spectral approach was followed. As a first step, the equivalent magnetic current distributions was Fourier-transformed in the transverse wavenumber plane $\mathbf{k}_\rho = k_x\hat{\mathbf{x}} + k_y\hat{\mathbf{y}}$, namely

$$\tilde{\mathbf{M}}(\mathbf{k}_\rho) = \iint_{\mathbb{R}^2} \mathbf{M}(\rho, \phi) e^{j(k_x x + k_y y)} dk_x dk_y \approx \sum_{n=1}^{N_p} \mathbf{M}_n e^{j\mathbf{k}_\rho \cdot \boldsymbol{\rho}_n} \rho_n, \tag{15}$$

with $\mathbf{M}_n$ denoting magnetic dipole moment of the n-th slot pair at $\boldsymbol{\rho}_n = (\rho_n, \phi_n)$ predicted by the MoM analysis. In Fig. 3, the co-polar component of the magnetic current distribution spectrum $|\tilde{\mathbf{M}}(\mathbf{k}_\rho) \cdot \hat{\mathbf{u}}^*_{RH}|$ is shown in the k_x–k_y transverse wavenumber plane at 57, 60, 63 GHz for CSW (a,b,c) and CITW (d,e,f) launchers, respectively. Since the aperture distributions are both almost azimuthally invariant, also the spectra are practically ϕ-independent in the form of spectral rings. In particular, because of the sampling in the radial direction due to the slot

Optics EXPRESS

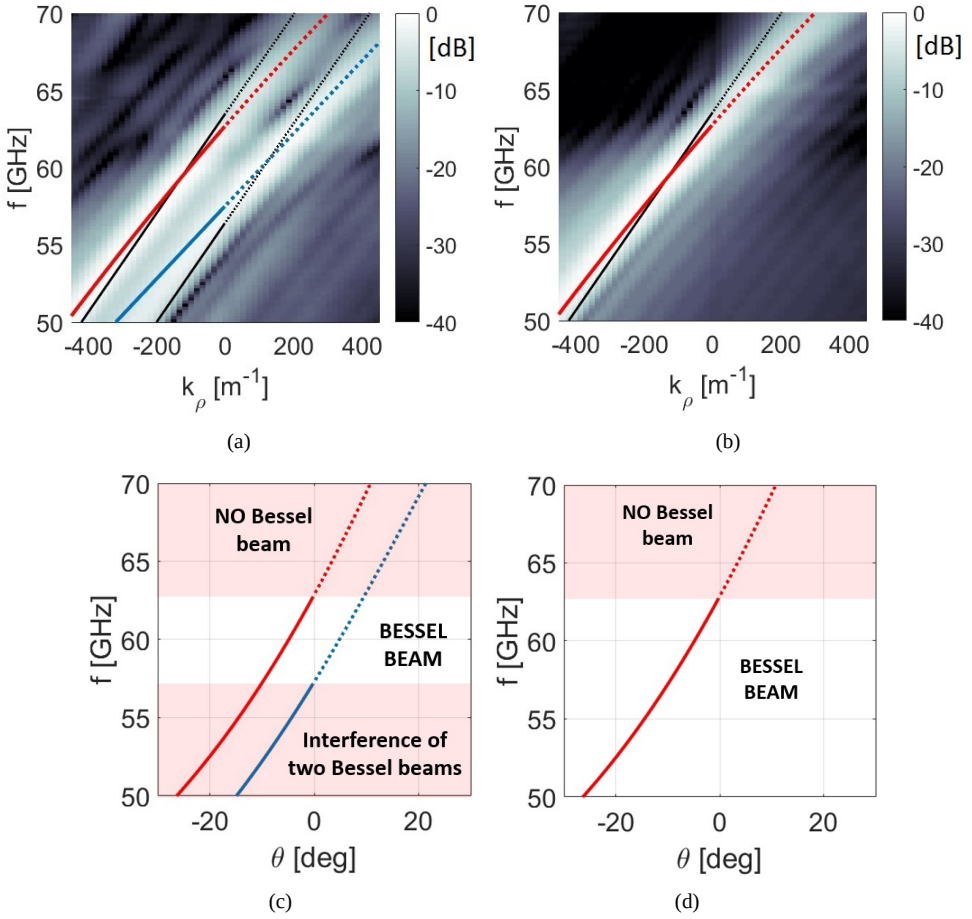

Fig. 4. (Background image) Co-polar traveling wave radial wavenumber (k_ρ) spectrum $|\tilde{\mathbf{M}}_0 \cdot \hat{\mathbf{u}}^*_{RH}|$ for varying frequency $f \in [50, 70]$ GHz, predicted by post-processing the MoM analysis for the (a) CSW and (b) CITW launchers. By collecting the background image maxima, the radial wavenumber dispersion diagram of the radiating $N = 0$ mode, obtained and compared against the approximate closed form model developed in Section 2 (black thin lines in (a) and (b)), is shown (red and blue thick lines). Dependence of the *axicon* angle θ on frequency for (c) CSW and (d) CITW launchers. The solid/dotted line style corresponds to the frequency range where the Bessel beam can/cannot be generated by the various wave constituents.

Optics EXPRESS

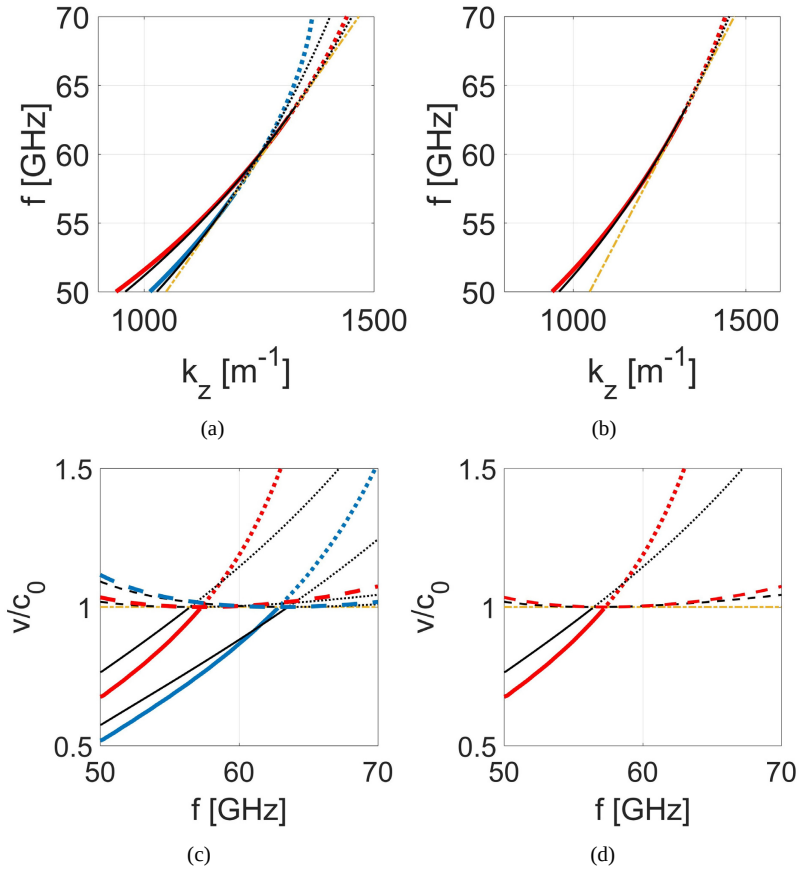

Fig. 5. Longitudinal wavenumber (k_z) dispersion diagram for varying frequency $f \in [50, 70]$ GHz, calculated by post-processing the MoM analysis for the (a) CSW and (b) CITW launchers (red and blue thick lines) and by using the theoretical model (black thin lines). Dependence of the phase velocity (dashed red and blue lines) and of the group velocity (solid/dotted red and blue lines) on frequency for (c) CSW and (d) CITW launchers, as predicted by the MoM analysis. The solid/dotted line style corresponds to the frequency range where the Bessel beam can/cannot be generated by the various wave constituents. The approximate theoretical counterparts (black lines) are also reported for comparison.

Optics EXPRESS

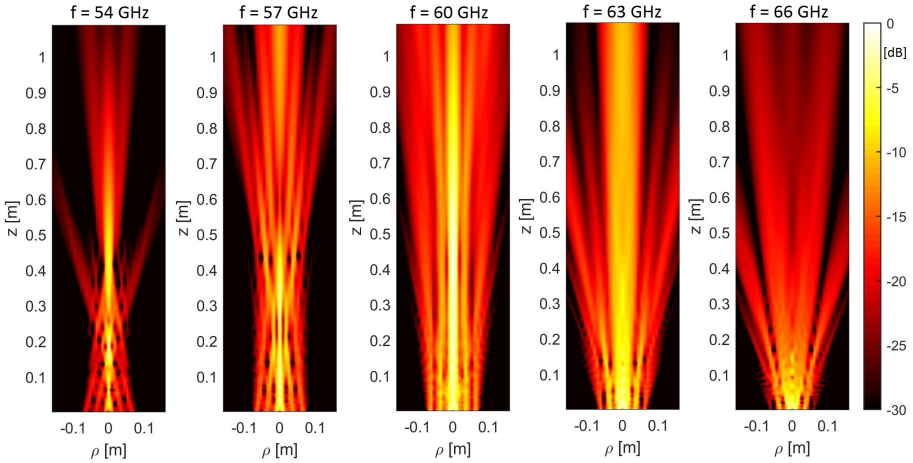

(a)

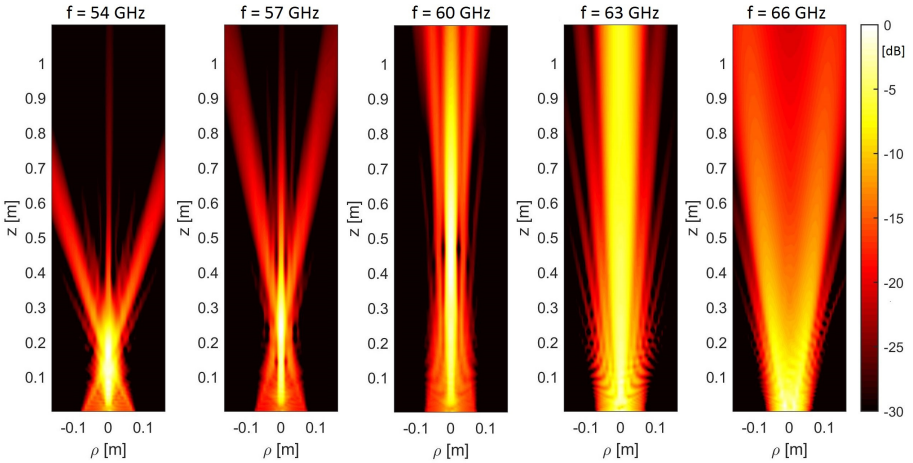

(b)

Fig. 6. Vertical ρz maps of co-polar component of the radiated electric field, by using the synthesized (a) CSW and (b) CITW aperture distributions, in the bandwidth $f \in [54, 66]$ GHz, respectively.

Optics EXPRESS

arrangement on a spiral with a step $\Delta S_B = 2\pi/\bar{k}_d$ for CSW and $\Delta S_H = 2\pi/(\bar{k}_d + \bar{k}_\rho)$ for CITW launchers, according to Floquet (or Bloch) Theorem, an infinite number of rings arises in the spectral domain. In addition, for the CSW launcher the slot amplitude modulation in Eq. (6) splits the "carrier" into two lateral spectral lines shifted by $\pm\bar{k}_\rho$. Therefore, the Floquet radial wavenumbers are $k_\rho^B = k_d + m\bar{k}_d \pm \bar{k}_\rho$ for CSW and $k_\rho^H = k_d + m(\bar{k}_d + \bar{k}_\rho)$ for CITW launchers, with $m \in \mathbb{Z}$. Among all the spectral replicas, only those for which $k_\rho^{B,H} \leq k_0$ contribute to the radiation (leaky waves), whereas the other are associated to surface waves, i.e., evanescent along the longitudinal z-direction. In the cases of CSW and CITW spectra of the equivalent magnetic current, only the $m = -1$ Floquet wave falls in the visible range (region inside red dashed lines in Fig. 3) and then contribute to the radiation of the Bessel beam. Namely, for $m = -1$ one finds $k_\rho^B = \Delta k_\rho \pm \bar{k}_\rho$ and $k_\rho^H = \Delta k_\rho - \bar{k}_\rho$, as discussed in Section 2.

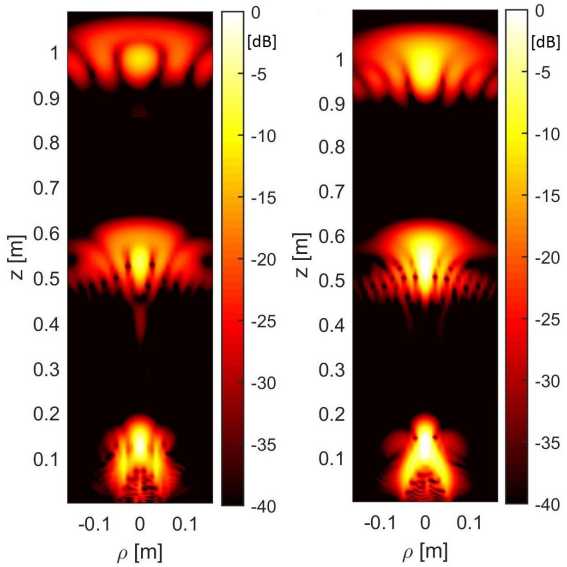

Fig. 7. Vertical $\rho - z$ field map showing the EM pulses generated at $t = 0.5, 2, 3.5$ ns by both CSW (left) and CITW (right) launchers. The spatial confinement along both longitudinal and transverse directions is clearly visible.

3.2. Radial wavenumber spectral analysis

A drawback in the k_x-k_y plane spectral representation is that outward and inward cylindrical wave constituents generating the Bessel beam cannot be recognized, since they exhibit the same spectral rings, as in Fig. 3. Then, in order to distinguish between them and calculate the radial wavenumber dispersion, it is of interest to expand the magnetic current distribution of both CSW and CITW launchers in terms of cylindrical traveling waves, namely

$$\tilde{\mathbf{M}}_N(k_\rho) = \int_0^{2\pi}\int_0^{+\infty} \mathbf{M}(\rho,\phi) H_N^{(1)}(k_\rho\rho) e^{jN\phi}\rho d\rho d\phi \approx \sum_{n=1}^{N_p} \mathbf{M}_n H_N^{(1)}(k_\rho\rho_n) e^{jN\phi_n}\rho_n, \quad (16)$$

being N_p the number of slot pairs. By evaluating the previous expression for both the CSW and CITW aperture distributions and for $N = 0, \pm 1$, due to the practical azimuthal symmetry achieved in these launchers, only the radial wavenumber associated to $N = 0$ significantly contributes to the radiated field. It is worth noting that the radial wavenumber defined in Eq.

Optics EXPRESS

(16) is connected to the transverse wavenumbers in Eq. (15) by $k_\rho = \pm\sqrt{k_x^2 + k_y^2}$, where $k_\rho > 0$ ($k_\rho < 0$) corresponds to outward (inward) waves. The co-polar component of the traveling wave spectrum $|\tilde{\mathbf{M}}_0(k_\rho) \cdot \hat{\mathbf{u}}^*_{RH}|$ is shown in Fig. 4 for various frequencies in the overall bandwidth $f \in [50, 70]$ GHz, for (a) CSW and (b) CITW launcher. The dispersion diagram for both the launchers was calculated by tracing the peaks of the traveling wave spectrum at any frequency and it is also shown in Figs. 4(a)–(b) (red and blue lines). As it is apparent, the dispersion diagram of the radiating mode $N = 0$ for the CSW launcher is composed by two wave constituents, namely at 60 GHz an inward ($k_\rho < 0$, red line) and an outward ($k_\rho > 0$, blue line) cylindrical waves, whereas the CITW launcher exhibits only one inward cylindrical wave constituent, as expected [26]. The solid/dotted line style corresponds to the frequency range where the Bessel beam can/cannot be generated by the various wave constituents. These numerically obtained dispersion diagrams are compared to their approximate estimation given in Section 2, marked with black lines in Figs. 4(a)–(b). The discrepancy between the closed form approximate model for the radial wavenumber dispersion estimation and that obtained by the numerical simulation is due to the fact that the former neglects the slot mutual coupling by using the simplified Bethe model [31], whereas the latter accounts for it. Therefore, the MoM can predict the correct radial wavenumber propagation of the feeding wave in the PPW when it is loaded by the slots, unlike the approximate model, in which the feeding wave is assumed to travel with the unperturbed wavenumber k_d. The closed form model qualitatively describes the phenomenon but the slope of the dispersion is slightly different. Moreover, in Figs. 4(c)–(d) the variation of axicon angle $\theta = \arcsin(k_\rho/k)$ is shown versus frequency in the considered bandwidth $f \in [50, 70]$ GHz.

In Figs. 5(a)–(b), the longitudinal wavenumber dispersion with frequency is shown, both for (a) CSW and (b) CITW launchers. The solid lines are associated to frequency ranges in which the Bessel beam cannot be generated by various wave constituents. In addition, in Figs. 5(c)–(d) the phase (dashed-dotted blue and red lines) and group velocities (solid blue and red lines), normalized to the speed of light in free-space, are depicted versus frequency for (c) CSW and (d) CITW launchers, respectively. As it is apparent, the phase velocity is *superluminal* in all the bandwidth, whereas the group velocity is always *subluminal* in the frequency ranges in which the Bessel beam can be generated (solid lines).

3.3. Monochromatic field maps

In order to analyze the generation of monochromatic Bessel beams in a broad band with respect to the central frequency, the co-polar component of the radiated electric field, i.e., $|\mathbf{E}(\mathbf{r}) \cdot \hat{\mathbf{u}}^*_{RH}|$, was calculated numerically for both CSW and CITW launchers, for various frequencies, and shown in Fig. 6. By recalling Eqs. (10)–(14), it is apparent that CSW (CITW) launchers can radiate a Bessel beam in the bandwidth $f \in \left[\bar{f}(1 - \sin\bar{\theta}/\sqrt{\epsilon_r}),\ \bar{f}(1 + \sin\bar{\theta}/\sqrt{\epsilon_r})\right] \approx [57, 63]$ GHz ($f \leq \bar{f}(1 + \sin\bar{\theta}/\sqrt{\epsilon_r}) \approx 63$ GHz). Below the lower frequency $f = 57$ GHz, the designed CSW launcher generates two interfering geometrical optics contributions, as can be noted in Fig. 4(a) at $f = 54$ GHz, whereas in the same frequency range CITW still generates a Bessel beam, as reported in Fig. 4(b) at $f = 54$ GHz. Hence, CITW in general exhibits a larger bandwidth with respect to CSW launchers. On the other hand, above the upper frequency $f = 63$ GHz neither CSW nor CITW launchers are able to radiate a Bessel beam and only diffraction contributes to the radiated field (see Figs. 4(a)–(b), $f = 66$ GHz). It is worth noting that at the upper limit of the bandwidth ($f = 63$ GHz), the non-diffractive range goes to infinity, hence both launchers behave as *afocal* systems, i.e. as standard antennas. The evaluation of the field maps in Fig. 6 with respect to frequency fits the dependence of the axicon angle θ on frequency described in the dispersion diagram of Figs. 4(c)–(d).

Optics EXPRESS

4. Time domain analysis of EM Gaussian pulses

A Gaussian frequency spectrum can be profitably used for the generation of EM pulses. Indeed, the transfer function of common RF transmitters can be well-approximated by a band-pass Gaussian filter. Moreover, the Fourier transform counterpart of a Gaussian function is still Gaussian, thus simplifying calculations involving Fourier spectra. Hence, we consider an unit power feeding Gaussian pulse carrying unitary power, whose analytical signal is

$$g^+(t) = \frac{e^{-\frac{t^2}{2\Sigma^2}} e^{j\omega_0 t}}{\pi^{1/4}\sqrt{\Sigma}}, \tag{17}$$

where Σ is the pulse standard deviation. Its Fourier spectrum is a Gaussian wave-packet

$$G(\omega) = \pi^{1/4}\sqrt{2\Sigma} e^{-(\omega-\omega_0)^2 \frac{\Sigma^2}{2}}, \tag{18}$$

whose bandwidth is proportional to $1/\Sigma$. The time-domain electric field generated when feeding a launcher by such a pulse can be calculated by properly superposing monochromatic Bessel beams as

$$\mathbf{e}^+(\rho, \phi, z; t) = \frac{1}{2\pi} \int_{-\infty}^{+\infty} G(\omega)\mathbf{E}(\rho, \phi, z; \omega) e^{j\omega t} d\omega. \tag{19}$$

4.1. Localized EM pulse maps

The proper superposition of all the monochromatic contributions to the radiated electric field $\mathbf{E}(\rho, z; \omega)$ over the entire considered bandwidth $f \in [50, 70]$ GHz, weighted by a Gaussian shape $G(\omega)$ of the form given in Eq. (18) with $\Sigma = 1/(4\pi)$ ns (corresponding to a 50% pulse duration of 187 ps and a 3 dB bandwidth of 3.32 GHz), allows for the generation of spatially localized EM pulses [1, 2]. In Fig. 7, the complex envelope magnitude of the co-polar component of the radiated electric field $|\mathbf{e}^+(\mathbf{r}) \cdot \hat{\mathbf{u}}^*_{RH}|$ is shown for CSW and CITW launchers at three different time instants, namely at $t = 0.5, 2, 3.5$ ns. When the pulse propagates along the longitudinal direction, it preserves its spatial confinement up to the non-diffractive range (i.e., $z_{dof} = \rho_{max} \cot\bar{\theta} \approx 90$ cm), whereas it starts spreading out beyond it. Therefore, EM pulses can be generated by means of CSW or CITW launchers.

5. Conclusion

In this paper, the broadband capabilities of two RLSA Bessel beam launchers, namely generated by CSW and CITW aperture distributions, have been analyzed. The simplified theoretical analysis of the EM field radiated by both the distributions have shown that CITW launchers can generate monochromatic Bessel beams over a larger bandwidth with respect to CSW ones. Moreover, two designs of CP Bessel beam launchers have been proposed by using an holographic approach, and an in-house MoM has been used for the analysis of the radiated EM field. In order to analyze the response of the launchers in a broad frequency band, the wavenumber dispersion has been estimated numerically. The last part of the paper have been focused on the possibility of generating spatially confined EM pulses by continuously superposing monochromatic Bessel beams over a certain bandwidth. The obtained results pave the way to efficiently design RLSA EM pulse launchers at microwaves/millimeter waves.